



SIMULATION OF NON-ISOTHERMAL NON-NEWTONIAN FLOW WITH MULTI-REGION THERMAL COUPLING

Mateus Palharini Schwalbert

Petróleo Brasileiro S.A. – Petrobras
Av. Tancredo Neves, 1367, Ed. Civil Trade, sala 908, CEP 41820-021, Salvador, BA, Brasil
m.palharini@yahoo.com.br

Paulo Laranjeira da Cunha Lage

Argimiro Resende Secchi
COPPE/UFRJ, Programa de Engenharia Química
Caixa Postal 68502, CEP 21941-972 Rio de Janeiro, RJ
paulo@peq.coppe.ufrj.br
arge@peq.coppe.ufrj.br

Abstract. *Several fluids used in oil and gas industry exhibit non-Newtonian behavior, with rheology strongly dependent on temperature. The transport of solid particles by these fluids and their flow rate and pressure drop relationships are important for oil well engineering. This work presents the development of a computational code for simulating the flow and heat transfer of non-Newtonian incompressible fluids, with temperature dependent rheology and multi-region heat transfer coupling, considering fluid and solid domains. The code was developed using the finite volume method, in the C++ programming language, using the CFD package OpenFOAM®, version 1.6-ext. The pressure-velocity coupling was carried out using the PIMPLE algorithm. The developed solver was named coupledMRNINNF (Coupled Multi-Region Non-Isothermal Non-Newtonian Foam). Results are presented for few problems, illustrating the importance of thermal coupling in vertical and horizontal oil wells and the effects of radial temperature gradient and drill string rotation on the pressure drop in an oil well.*

Keywords: *oil well hydraulics, CFD, OpenFOAM, non-Newtonian fluids.*

1. INTRODUCTION

The existence of increasingly challenging scenarios in the oil and gas exploration and production implies their operation with small economical margins, which requires the largest possible accuracy in well design. Oil well drilling is an extremely costly operation in which an excessive error might turn operations uneconomical or technically unfeasible.

One important aspect in drilling operations is the flow of the drilling fluids which is responsible for the transport of the cuttings and for the pressure inside the well, which determines the well mechanical stability and operational safety. These fluids exhibit non-Newtonian behavior with a highly temperature-dependent rheology. Therefore, the flow pressure losses depend on the well temperature field. Even the fluid density, which determines the hydrostatic pressure field, depends slightly on the temperature and pressure fields.

However, the heat transfer analysis in the flow of drilling fluids is usually either not considered or estimated through one-dimensional models. These simple models commonly employ correlations for the heat transfer coefficients which have been developed for Newtonian fluids. Some of these models are presented in Raymond (1969), Holmes and Swift (1970), Keller *et al.* (1973), Wooley (1980), Hoang and Somerton (1981), Marshall and Bentsen (1982), Corre *et al.* (1984), Beirut (1991), Garcia *et al.* (1998), Aranha *et al.* (2011), Aranha *et al.* (2008) and Waldmann *et al.* (2009). They solve a one-dimensional energy balance for an axial temperature profile, fully uncoupled with the fluid flow equations.

Other cases of non-Newtonian fluid flow in long pipes subject to non-isothermal conditions occur in oil well engineering, such as operations for well stimulation and for pumping of cement slurries.

In order to achieve a better comprehension of these phenomena, this work developed a computational code for simulating the flow and heat transfer of non-Newtonian incompressible fluids with temperature dependent rheology and multi-region conjugated heat transfer coupling.

2. METHODOLOGY

A mathematical model using computational fluid dynamics was developed and implemented in the CFD package *OpenFOAM*® (Open-Source Field Operation and Manipulation), version 1.6-ext. The model description and some implementation details are given in the following.

2.1 Mathematical Model

The solver can consider several fluid and solid domains. Fluid and solid domains were modeled using a different set of governing equations. For a fluid domain, the conservation equations for momentum, mass and energy were solved for the fields of velocity, pressure and temperature, considering an incompressible non-Newtonian fluid. For the solid domains, only the energy equation was solved for the temperature.

Fluid domain conservation equations. The continuity equation for an incompressible fluid is simply:

$$\nabla \cdot \mathbf{U} = 0 \quad (1)$$

where \mathbf{U} is the fluid velocity vector. The momentum conservation equation is given by:

$$\rho \frac{\partial \mathbf{U}}{\partial t} + \rho \nabla \cdot (\mathbf{U}\mathbf{U}) + \nabla \cdot \boldsymbol{\tau} = -\nabla p + \rho \mathbf{g} \quad (2)$$

where t is the time, $\boldsymbol{\tau}$ is the viscous stress tensor, ρ is fluid density, p is the pressure, and \mathbf{g} is the gravitational acceleration.

The viscous stress depends on the rheological model used to describe the fluid. Different rheological models were implemented, all belonging to the generalized Newtonian fluid model, given by Eq. (3),

$$\boldsymbol{\tau} = -\eta(\dot{\gamma})\dot{\boldsymbol{\gamma}} \quad (3)$$

which represents the viscous stress tensor as proportional to the rate of strain tensor $\dot{\boldsymbol{\gamma}}$, defined by

$$\dot{\boldsymbol{\gamma}} = \nabla \mathbf{U} + (\nabla \mathbf{U})^T \quad (4)$$

whose proportionality coefficient is called the apparent viscosity and represented by $\eta(\dot{\gamma})$, being an algebraic function of the scalar rate of strain defined by:

$$\dot{\gamma} = |\dot{\boldsymbol{\gamma}}| = \sqrt{\frac{1}{2} \dot{\boldsymbol{\gamma}} : \dot{\boldsymbol{\gamma}}} = \sqrt{\frac{1}{2} \sum_i \sum_j \dot{\gamma}_{ij} \dot{\gamma}_{ji}} \quad (5)$$

Some different generalized Newtonian fluid models were implemented, such as the power-law model by Ostwald and de Waele,

$$\boldsymbol{\tau} = -k\dot{\gamma}^{n-1}\dot{\boldsymbol{\gamma}}, \quad (6)$$

the Herschel-Bulkley model,

$$\left\{ \begin{array}{l} \boldsymbol{\tau} = -\eta(\dot{\gamma})\dot{\boldsymbol{\gamma}} \\ \eta(\dot{\gamma}) = \frac{\tau_o + k\dot{\gamma}^n}{\dot{\gamma}} \end{array} \right\} \text{ for } |\boldsymbol{\tau}| > \tau_o, \quad \left\{ \begin{array}{l} \dot{\boldsymbol{\gamma}} = \mathbf{0} \\ \eta = \infty \end{array} \right\} \text{ for } |\boldsymbol{\tau}| \leq \tau_o, \quad (7)$$

the Cross model,

$$\boldsymbol{\tau} = - \left[\eta_\infty + \left(\frac{\eta_o - \eta_\infty}{1 + (\lambda\dot{\gamma})^n} \right) \right] \dot{\boldsymbol{\gamma}}, \quad (8)$$

the Carreau model,

$$\boldsymbol{\tau} = - \left[\eta_\infty + (\eta_o - \eta_\infty) (1 + (\lambda\dot{\gamma})^2)^{\frac{n-1}{2}} \right] \dot{\boldsymbol{\gamma}}, \quad (9)$$

and the Carreau-Yasuda model,

$$\boldsymbol{\tau} = - \left[\eta_\infty + (\eta_o - \eta_\infty) (1 + (\lambda\dot{\gamma})^a)^{\frac{n-1}{a}} \right] \dot{\boldsymbol{\gamma}} \quad (10)$$

In addition, the Newtonian model, given by Eq. 11, was also implemented.

$$\boldsymbol{\tau} = -\mu\dot{\boldsymbol{\gamma}} \quad (11)$$

All these equations are suited for incompressible and isothermal fluids, and k , n , τ_o , λ , a , η_o and η_∞ are all adjustable parameters and μ is the dynamic viscosity of a Newtonian fluid.

The rheology dependence on temperature was modeled according to Tanner (2000):

$$\tau(\dot{\gamma}, T) = \frac{T}{T_o} \tau(a_T \dot{\gamma}, T_o) \quad (12)$$

where T is temperature, T_o is a reference temperature, and a_T is a factor that describes the temperature dependence, which in the case of well engineering fluids might be given by:

$$a_T = \exp \left[\frac{\Delta \tilde{H}}{R} \left(\frac{1}{T} - \frac{1}{T_o} \right) \right] \quad (13)$$

where $\Delta \tilde{H}$ is an adjustable parameter and R is the universal gas constant.

Substituting the viscous stress tensor in Eq. (2) and dividing by the fluid density, we derive the following equation for the velocity field which was then implemented in OpenFOAM®.

$$\frac{\partial \mathbf{U}}{\partial t} + \nabla \cdot (\mathbf{U}\mathbf{U}) - \nabla \cdot (\nu \nabla \mathbf{U}) = -\frac{1}{\rho} \nabla p + \mathbf{g} + \nabla \nu \cdot (\nabla \mathbf{U})^T \quad (14)$$

where ν is the apparent kinematic viscosity, given by the apparent viscosity divided by the fluid density $\nu = \eta(\dot{\gamma})/\rho$.

The energy conservation equation was expressed as:

$$\rho C_p \frac{\partial T}{\partial t} + \rho C_p \nabla \cdot (\mathbf{U}T) = \nabla \cdot (k \nabla T) - \boldsymbol{\tau} : \nabla \mathbf{U} \quad (15)$$

where C_p is the specific heat capacity at constant pressure, which was assumed to be constant, and k is thermal conductivity.

Solid domain conservation equations. For a solid domain, only the energy conservation equation must be solved. In the case of a static solid, it reduces to the transient heat diffusion equation:

$$\rho C_p \frac{\partial T}{\partial t} = \nabla \cdot (k \nabla T) \quad (16)$$

In the more general case of a solid moving in relation to the adopted reference frame, the energy equation must contain the advective term, that is:

$$\rho C_p \frac{\partial T}{\partial t} + \rho C_p \nabla \cdot (\mathbf{U}T) = \nabla \cdot (k \nabla T) \quad (17)$$

where the solid velocity field does not need to be solved for, because it is given as an imposed rigid body translation and/or rotation velocity. In the case of a rotating solid with axisymmetry, the advective term cancels out.

Fluid-solid boundary conditions. The thermal coupling at the fluid-solid interfaces is carried out by imposing temperature and heat flux continuity at these boundaries. In this section, the s and f subscripts are used to the solid and fluid fields and properties, respectively. Being \mathbf{x} the position vector and \mathbf{x}_i its value at the fluid-solid interface, the boundary conditions that implement the thermal coupling are given by:

$$\lim_{\mathbf{x} \rightarrow \mathbf{x}_i} T_s = \lim_{\mathbf{x} \rightarrow \mathbf{x}_i} T_f \quad (18)$$

$$k_s \hat{\mathbf{n}} \cdot \nabla T_s \Big|_{\mathbf{x} \rightarrow \mathbf{x}_i} = k_f \hat{\mathbf{n}} \cdot \nabla T_f \Big|_{\mathbf{x} \rightarrow \mathbf{x}_i} \quad (19)$$

where $\hat{\mathbf{n}}$ is the unitary vector normal to the boundary surface.

2.2 Implementation

The computational implementation was carried out using the CFD package *OpenFOAM*®, version 1.6-ext. The rheological models were implemented in a new library named *transportModelsNonIsothermal*, which is a modification of the existing library *transportModels*. The changes in the existing library consisted of the addition of the temperature field dependence in the parameters of the viscosity models, the inclusion of the Carreau-Yasuda model, and the modification of the rate of strain tensor definition, which became calculated as given by Eq. (5). It is worth noting that the rate of strain tensor was explicitly calculated.

For the solution of the heat transfer in the flow of a non-Newtonian fluid, a single-domain solver was developed. It was called *NINNF*, which stands for *Non-Isothermal Non-Newtonian Foam*. It is a modification of the solver *nonNewtonianIcoFoam* that exists in *OpenFOAM®*. The main modification was the addition of the energy equation solution for the temperature field with temperature-dependent rheological models. In addition, the following modifications were carried out:

- addition of the term $[\nabla\nu \cdot (\nabla U)^T]$ in the right-hand side of the momentum conservation equation, Eq. (14), which was neglected in the original solver;
- activation of the mesh non-orthogonality corrections for the solution of the momentum and energy equations;
- modification of the pressure-velocity coupling algorithm from PISO, which is used in *nonNewtonianIcoFoam*, to PIMPLE, which is used in the existing solver *pimpleFoam* from *OpenFOAM®*);
- implementation of a mixed convergence criterion based on the maximum of the pressure field change between successive iterations of the solution algorithm.

The last two modification were made in order to improve the convergence behavior of the pressure equation solution, which was clearly the most difficult step for the overall algorithm convergence in the performed tests.

For the simulation of the fluid-solid conjugated heat transfer in the flow of a non-Newtonian fluid, a multi-region solver was created. It was named *coupledMRNINNF*, which stands for *coupled Multi-Region Non-Isothermal Non-Newtonian Foam*. This was developed from the *NINNF* solver by splitting the mesh into multiple domains of two types: solid and fluid, similarly to what is done in the solver *chtMultiRegionFoam* that exists in *OpenFOAM®*, version 1.6-ext. It is possible to define two or more fluid domains with different properties and rheological models. The definition of multiple solid domains with different properties is also possible.

In the fluid domains, the heat transfer problem in the flow of an incompressible non-Newtonian fluid with temperature dependent rheology was solved for pressure, velocity and temperature, exactly as in the *NINNF* solver. In the solid domains, the solution of the transient heat diffusion equation, Eq. (16), was implemented. For the cases of interest in the present work, the advective term in Eq. (17) has no contribution. However, if necessary, its implementation from a given velocity field is trivial.

The heat transfer coupling between fluid and solid domains was carried out using the boundary conditions expressed by Eqs. (18) and (19), which were previously implemented in *OpenFOAM®*, version 1.6-ext. This pair of boundary conditions was named *solidWallMixedTemperatureCoupled*. In its usage, the user must specify the temperature and thermal conductivity fields from both domains which form the interface. Other possible boundary conditions for the solid-fluid interface are available, such as *solidWallTemperatureCoupled*, *solidWallHeatFluxTemperature* and *solidWallHeatFluxTemperatureCoupled*.

For the convergence of the solution in the multiple domains, an overall convergence loop was included. The usage of *coupledMRNINNF* is a bit different from other solvers available in *OpenFOAM®*, version 1.6-ext. A usage tutorial is available at Schwalbert (2013).

3. RESULTS

3.1 Code verification

In order to verify the solvers *NINNF* and *coupledMRNINNF*, tests with simplified problems that could be simulated with existing *OpenFOAM®*(version 1.6-ext) solvers were conducted. Therefore, code verification was carried out by comparing the simulated results obtained using these solvers and those developed in this work.

For verifying the fluid dynamics solution implemented in both codes, the isothermal flow of Newtonian and non-Newtonian fluids were used. The solutions of some test cases obtained using the *NINNF* were compared to the *nonNewtonianIcoFoam* solution, for non-Newtonian fluid models, and to the *icoFoam* solution, for a Newtonian fluid. For all test cases, the *NINNF* results were in excellent agreement to the results of the other solvers, verifying this part of the code also implemented in the *coupledMRNINNF* solver.

The solution of the heat transfer problem in the flow of a fluid was verified by imposing the steady-state velocity field in the flow in a circular duct obtained from the *NINNF* solver into the *scalarTransportFoam* solver present in *OpenFOAM®*, that solves the transport equation for a passive scalar which, in this case, is the temperature. The agreement between the temperature profiles obtained directly by the *NINNF* solver and by using the strategy described above was very good.

For the verification of the heat transfer coupling at the interface of different domains, a heat transfer problem using two solid domains was used. It consists of the one-dimensional heat transfer through two solid plates with a common interface and with fixed temperatures at their other faces (see Fig. 1). The steady-state solution given by the *coupledMRNINNF*

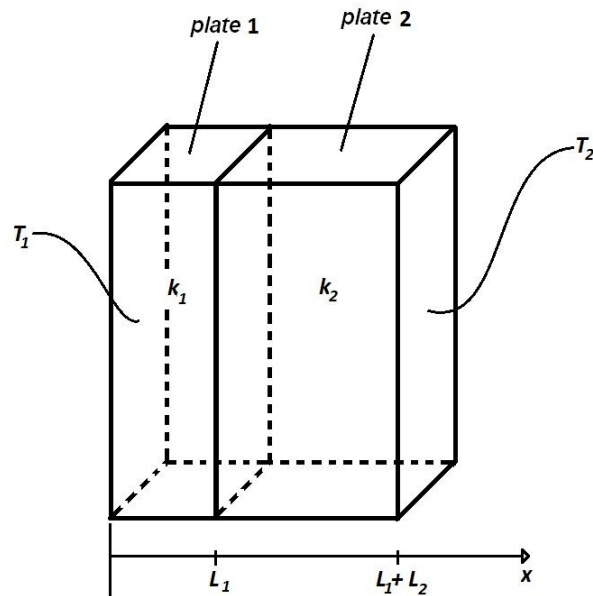


Figure 1. System of two contacting solid plates for simulating the heat transfer coupling at the interface.

solver was compared with the analytical solution for this problem:

$$T(x) = \begin{cases} T_1 + \frac{T_i - T_1}{L_1}x, & 0 \leq x \leq L_1 \\ T_i + \frac{T_2 - T_i}{L_2}(x - L_1), & L_1 \leq x \leq L_1 + L_2 \end{cases} \quad (20)$$

where the solid plate 1 has thermal conductivity k_1 , begins at $x = 0$ and ends at $x = L_1$, the solid plate 2 has thermal conductivity k_2 , begins at $x = L_1$ and ends at $x = L_1 + L_2$, T_1 is the temperature at $x = 0$, T_2 is the temperature at $x = L_1 + L_2$ and T_i is the temperature at the interface, given by Eq. (21). Both plates are infinite in the directions orthogonal to the x axis.

$$T_i = \frac{k_2 L_1 T_2 + k_1 L_2 T_1}{k_1 L_2 + k_2 L_1} \quad (21)$$

Figure 2 shows the results for the case with $T_1 = 200K$, $T_2 = 400K$, $L_1 = L_2 = 0.01m$, $k_1 = 3k_2 = 3000WK^{-1}m^{-1}$ and $k_2 = 1000WK^{-1}m^{-1}$. Figure 3 shows the results for the case with $T_1 = 200K$, $T_2 = 400K$, $L_1 = 0.01m$, $L_2 = 2L_1 = 0.02m$, $k_1 = 500WK^{-1}m^{-1}$ and $k_2 = 3k_1 = 1500WK^{-1}m^{-1}$.

In Figs. 2 and 3, the continuous line represents the analytical solution while the symbols show the numerical results. It can be seen that the results are in very good agreement, which verifies the code for the thermal coupling between domains.

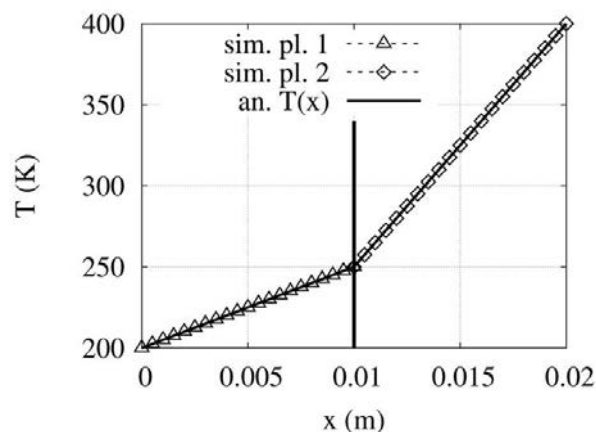


Figure 2. Heat transfer coupling at the interfaces of two solid domains with $L_1 = L_2$ and $k_1 = 3k_2$: comparison between analytical (solid line) and numerical (symbols) solutions.

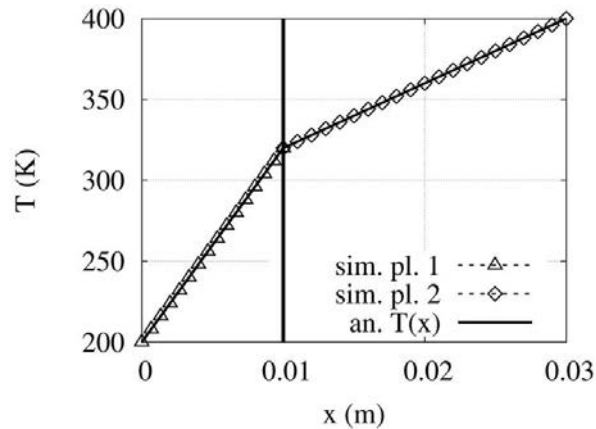


Figure 3. Heat transfer coupling at the interfaces of two solid domains with $L_2 = 2L_1$ and $k_2 = 3k_1$: comparison between analytical (solid line) and numerical (symbols) solutions.

3.2 Application cases

The examples of the application of the *coupledMRNINNF* solver consider the heat transfer in the flow of a non-Newtonian fluid in an oil well section with 700 meter of length. The corresponding geometry is shown in Fig. 4 and the geometric data is listed in Table 1.

This example represents the drilling process of an oil well. It is assumed that the drill is operating at the bottom of the well section represented in Fig. 4. It is not geometrically represented, but its effect on the heat transfer problem was considered. However, the drilling bit jets were not considered in the simulations.

The drilling fluid flows down the drill string (internal concentric cylindrical tube in Fig. 4), flows through the drill bit and then rises in the annular region between the drill string wall and the well walls, while the drill string rotates. The well walls were considered at the geothermal temperature profile and, therefore, the annulus fluid is heated, from which the heat is transferred to the drill string solid steel, which then heats the drill string internal fluid.

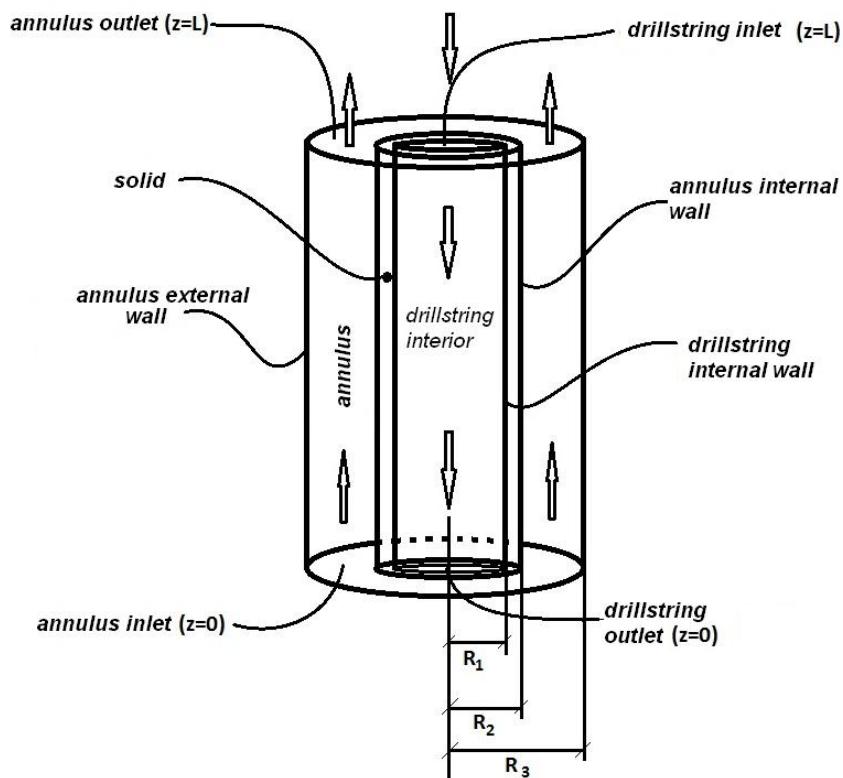


Figure 4. Geometry and boundaries of the oil well section.

Table 1. Geometric characteristics of the oil well section

Variable	Value (m)	Value in field units
length	700	700 <i>m</i>
external well diameter	0.2159	8½ <i>in</i>
external drill string diameter	0.127	5 <i>in</i>
internal drill string diameter	0.1086	4.276 <i>in</i>

The fluid is heated during its passage by the well bottom due to the heat generated by the drilling process. Thus, it was necessary to couple the temperature of the drill string and annulus fluids at the well bottom. That was implemented directly at the solver code. A perfect mixture was assumed at the well bottom, so that the heat added to the fluid in this region increases its temperature from the drill string outlet temperature up to the temperature at the annulus inlet.

The physical and transport properties used in the simulations are those listed in Table 2. The rheology was modeled by the Carreau-Yasuda model, whose parameters were estimated from measurements of an actual oil-based drilling fluid. Different fluid flow rates and drill string rotations were used in the simulations, as presented in Table 3. It also lists the fluid average axial velocity in the drill string ($U_{z,av,ds}$) and in the annulus ($U_{z,av,an}$), as well as the drill string rotation angular velocities.

In the following, several simulation results for the steady-state conditions are reported. A mesh convergence analysis was carried out and the presented results were converged to a large degree of accuracy. Figure 5 shows the simulated annulus radial temperature profiles obtained at the depth 200 *m* above the bottom, when there is no drill string rotation and for the three considered flow rates. Figure 6 shows similar results but at the depth 700 *m* above the bottom. Finally, Fig. 7 shows the annulus temperature profiles at 400 *m* above the bottom for the flow rate of 300 *gpm* and the four drill string rotations.

It can be observed that the rotation makes little or no influence in the radial temperature profile and the drilling fluid heating is larger at lower flow rates. Besides, for the range of the simulated conditions, the fluid inside the drill string suffers almost no heating, because the thermal boundary layer does not reach the drill string in the 700 *m* extent.

Figure 8 shows the radial profiles of the axial component of the fluid velocity in the annulus (U_z) at the depth 400 *m* above the bottom for the four drill string rotation speeds and the flow rate of 300 *gpm*. Figure 9 shows similar results but for the flow rate of 500 *gpm*. From these figures, it is clear that the axial velocity is little affected by the rotation.

Figure 10 shows the radial profiles of the tangential component of the fluid velocity in the annulus (U_θ) at the depth 400 *m* above the bottom for the four drill string rotation speeds and the flow rate of 500 *gpm*. As expected, the tangential velocity decreases from the drill string wall to the well wall, having a region far from both walls where the fluid almost achieves a solid rotation, that is, with constant angular velocity. This results from the non-Newtonian character of the fluid.

Table 2. Physical properties used in the simulations

Material	Property	Value
Drilling Fluid	ρ (kg/m^3)	1150.33
	C_p ($Jkg^{-1}K^{-1}$)	2265.15
	k ($WK^{-1}m^{-1}$)	0.286
Drill string Steel	ρ (kg/m^3)	7833
	C_p ($Jkg^{-1}K^{-1}$)	467.7
	k ($WK^{-1}m^{-1}$)	54

Table 3. Operational conditions used in the simulations

Parameters	Values			
	S.I. units (m^3/s)	field units (<i>gpm</i>)	$U_{z,av,an}$ (<i>m/s</i>)	$U_{z,av,ds}$ (<i>m/s</i>)
Flow rate	0.0189	300	0.79	2.04
	0.0252	400	1.05	2.72
	0.0315	500	1.32	3.40
Rotation	rotation speed (<i>rpm</i>)		angular velocity (<i>rad/s</i>)	
	0		0	
	50		5.24	
	100		10.47	
	150		15.71	

M. P. Schwalbert, P. L. C. Lage and A. R. Secchi
Simulation of non-isothermal non-Newtonian flow with multi-region thermal coupling

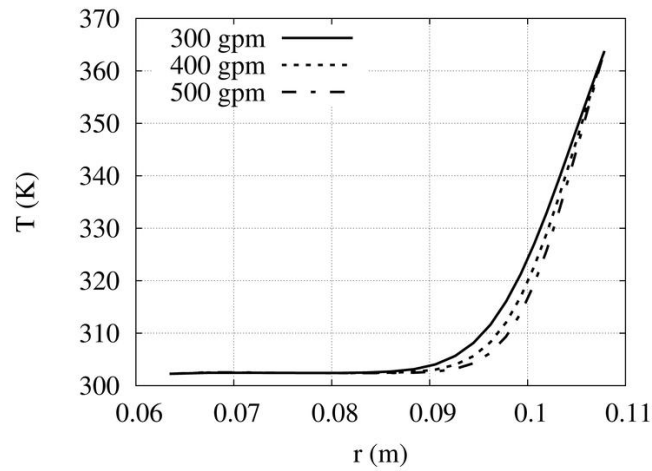


Figure 5. Annulus radial temperature profiles at three flow rates with no drill string rotation at 200 *m* above the well bottom.

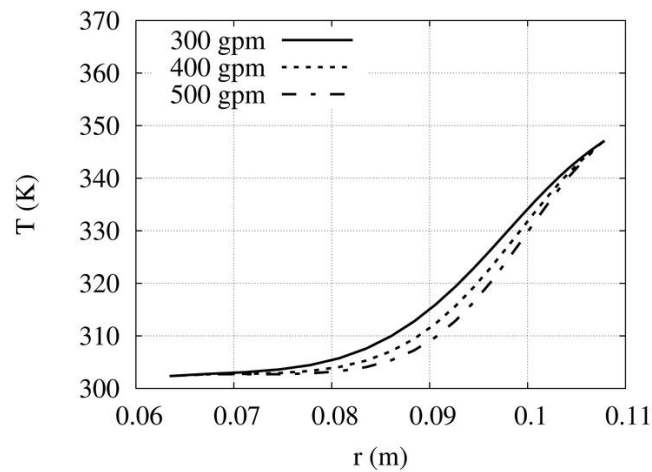


Figure 6. Annulus radial temperature profiles at three flow rates with no drill string rotation at 700 *m* above the well bottom.

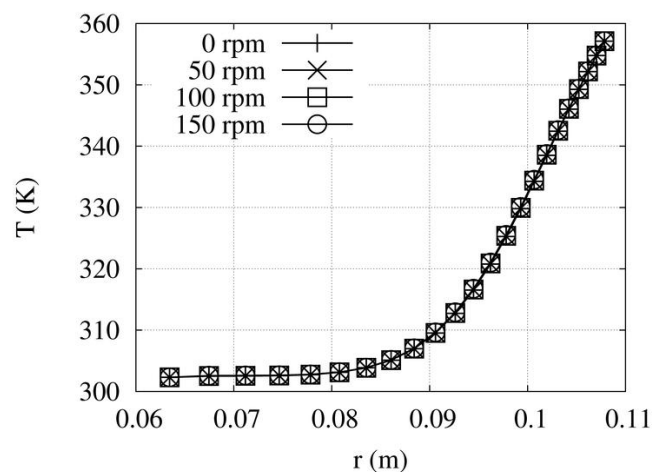


Figure 7. Annulus radial temperature profiles at four rotation speeds, with the drilling fluid flow rate of 300 *gpm* at 400 *m* above the well bottom.

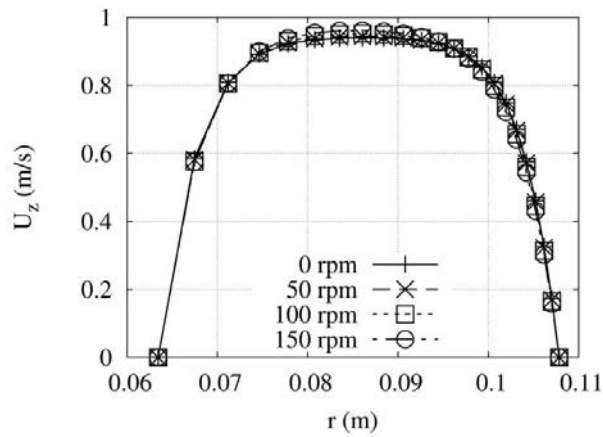


Figure 8. Annulus Radial profiles of the fluid velocity axial component at four rotation speeds, with the drilling fluid flow rate of 300 *gpm* at 400 *m* above the well bottom.

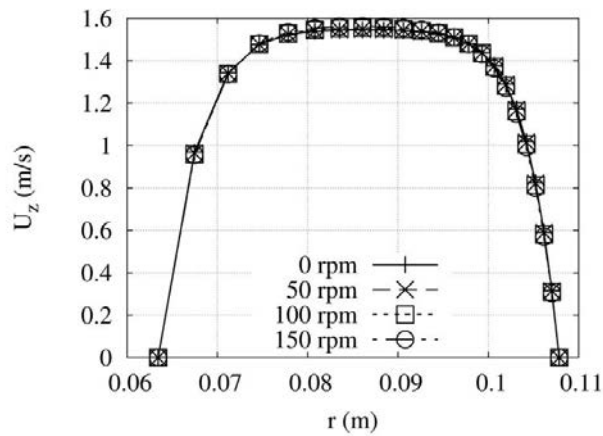


Figure 9. Annulus radial profiles of the fluid velocity axial component at four rotation speeds, with the drilling fluid flow rate of 500 *gpm* at 400 *m* above the well bottom.

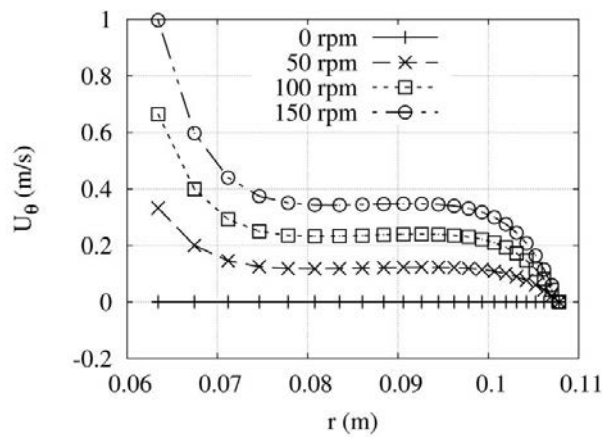


Figure 10. Annulus radial profiles of the fluid velocity tangential component at four rotation speeds, with the drilling fluid flow rate of 500 *gpm* at 400 *m* above the well bottom.

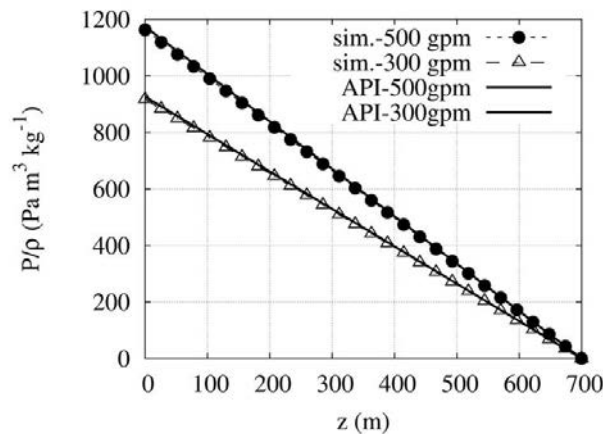


Figure 11. Pressure loss along the 700 *m* for the isothermal flow with no rotation at two flow rates, and comparison with the results of the correlation recommended by API (2009).

Figure 11 shows the pressure loss along the 700 *m* extent for the isothermal flow with no rotation, for flow rates of 300 and 500 *gpm*. It also shows the corresponding pressure losses calculated using the correlation recommended by API (2009), showing that the correlation is quite good when there is no rotation and no heating of the fluid.

Figure 12 shows the pressure losses along the 700 *m* extent for the non-isothermal flow with rotation, for the four drill string rotation speeds and the flow rate of 300 *gpm*. It shows that, in this range of parameters, the increase in the rotation speed reduces the pressure loss. Figure 13 shows similar results for the flow rate of 400 *gpm*. Comparing these results with those of the correlation recommended by API (2009), also shown in these figures, it can be seen that the presence of rotation of the drill string or the heat transfer in the flow increases the prediction error of this correlation.

As the heating of the drilling fluid was small in the considered section of a vertical well, a simulation was carried out for a horizontal well of 700 *m* long, entirely in the region of the higher depth and, therefore, higher temperature of the previous simulations. Figure 14 shows the radial profiles of the temperature throughout the three domains (drill string internal fluid, solid steel and annulus fluid) at different axial positions for a flow rate of 300 *gpm* and rotation speed of 100 *rpm*. It can be seen that even in this case the heating in the 700 *m*-long section was not enough to rise the drill string fluid temperature by a significant amount.

4. CONCLUSIONS

A mathematical model for the conjugated heat transfer in the flow of an incompressible non-Newtonian fluid with temperature-dependent rheological model was developed and implemented in an open-source computational code. The resulting solver can handle any number of fluid and solid domains. The code was verified and used to simulate some cases that represent the heat transfer problem in the drilling process of an oil well, obtaining satisfactory results. These examples proved the usefulness of this code in improving the understanding of the flow with heat transfer phenomena that occurs in several operations of the oil well engineering.

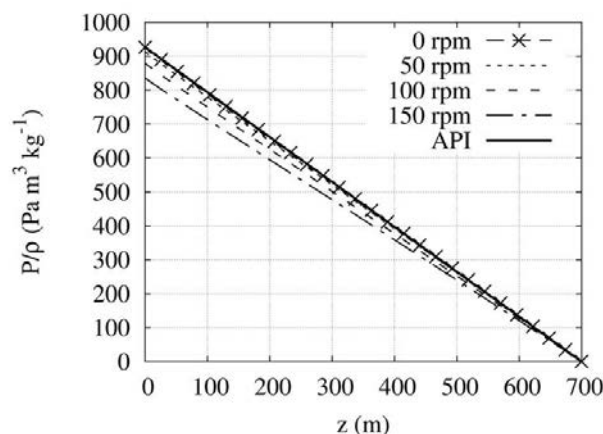


Figure 12. Pressure loss along the 700 *m* for the non-isothermal flow at the four drill string rotation speeds at the flow rate of 300 *gpm*.

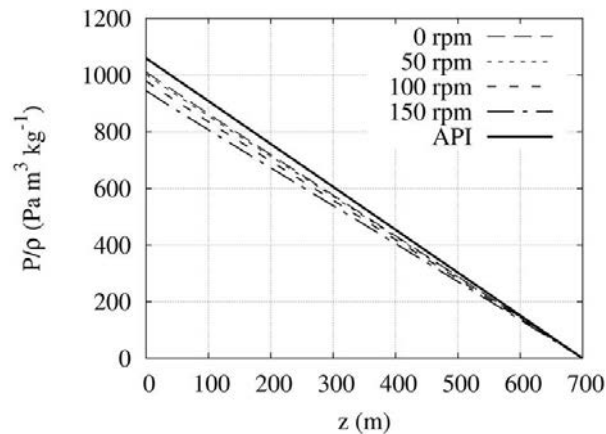


Figure 13. Pressure loss along the 700 m for the non-isothermal flow at the four drill string rotation speeds at the flow rate of 400 gpm.

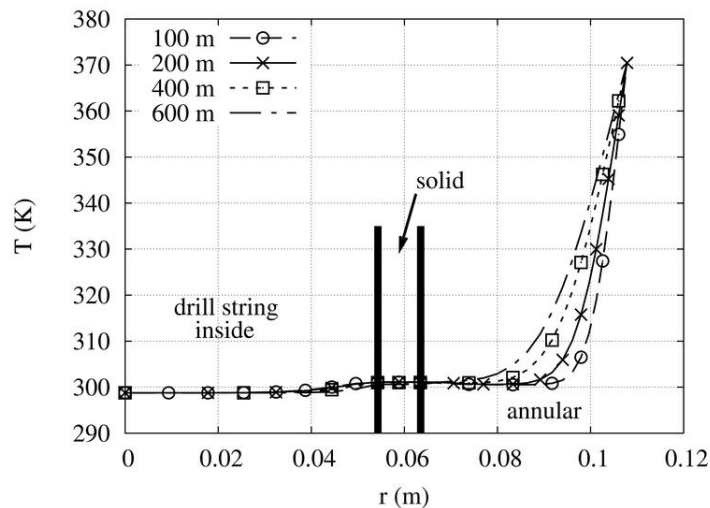


Figure 14. Horizontal well radial temperature profiles in the three domains at different axial positions.

5. ACKNOWLEDGEMENTS

Paulo L. C. Lage acknowledges the financial support from CNPq, grants nos. 302963/2011-1 and 478589/2011-5, and FAPERJ, grant no. E-26/111.361/2010.

Argimiro R. Secchi acknowledges the financial support from CNPq, grants 304907/2009-0 and 480040/2010-9.

6. REFERENCES

- API, 2009. "API recommended practice 13d – rheology and hydraulics of oil-well drilling fluids". In: Report SC 13/WG 7, American Petroleum Institute, Washington, D.C., USA.
- Aranha, P.E., Gandelman, R.A., Waldmann, A., Moura, H.C., Martins, A.L. and Aragao, A.F.L., 2008. "Avaliação do efeito de temperatura nos parâmetros reológicos dos fluidos Petrobras". In *III Seminário de Fluidos de Perfuração e Completação – Acesso Restrito*. Rio de Janeiro, RJ, Brasil.
- Aranha, P.E., Martins, A.L., Miranda, C.R., Campos, G., Dannenhauer, C.E., Rezende, M.S., Ribeiro, P.H.R. and Manoel, E.T., 2011. "Simentar 1.0 - simulador integrado de cimentação - inclusão dos módulos térmico e de circulações intermediárias". Relatório Parcial – Acesso Restrito – RT PCP 001 /11, CENPES - Petróleo Brasileiro S. A., Rio de Janeiro.
- Beirute, R.M., 1991. "A circulating and shut-in well temperature profile simulator". *Journal of Petroleum Technology*, pp. 1140–1146.
- Corre, B., Eymard, R. and Guenot, A., 1984. "Numerical computation of temperature distribution in a wellbore while drilling". In *Proceedings of the SPE 59th Annual Technical Conference and Exhibition*. Houston, Texas, EUA, pp. 1–24.

M. P. Schwalbert, P. L. C. Lage and A. R. Secchi
Simulation of non-isothermal non-Newtonian flow with multi-region thermal coupling

- Garcia, A., Hernandez, I., Espinosa, G. and Santoyo, E., 1998. “Temlopi: a thermal simulator for estimation of drilling mud and formation temperatures during drilling of geothermal wells”. *Computers and Geosciences*, Vol. 24, No. 5, pp. 465–477.
- Hoang, V.T. and Somerton, W.H., 1981. “Effect of variable thermal conductivity of the formations on the fluid temperature distribution in the wellbore”. In *Proceedings of the SPWLA TWENTY-SECOND ANNUAL LOGGING SYMPOSIUM*. pp. 1–24.
- Holmes, C.S. and Swift, S.C., 1970. “Calculation of circulating mud temperatures”. *Journal of Petroleum Technology*, pp. 670–674.
- Keller, H.H., Couch, E.J. and Berry, P.M., 1973. “Temperature distribution in circulating mud columns”. *Society of Petroleum Engineers Journal*, pp. 23–30.
- Marshall, D.W. and Bentsen, R.G., 1982. “A computer model to determine the temperature distributions in a wellbore”. *The Journal of Canadian Petroleum*, pp. 63–75.
- Raymond, L.R., 1969. “Temperature distribution in a circulating drilling fluid”. *Transactions*, Vol. 246, pp. 333–341.
- Schwalbert, M.P., 2013. *Simulação de Escoamentos Não Newtonianos Não Isotérmicos e Sua Aplicação à Engenharia de Poços de Petróleo*. M.Sc. dissertation, COPPE/UFRJ, Rio de Janeiro, RJ, Brasil.
- Tanner, R.I., 2000. *Engineering Rheology*. Oxford University Press, Oxford, 1st edition.
- Waldmann, A., Gandelman, R.A., Aranha, P.E., Santos, D.M., Martins, A.L., Costa, S.S. and Wohlers, D., 2009. “Simcarr 2009”. Relatório Parcial – Acesso Restrito – RT TEP 002-09, CENPES - Petróleo Brasileiro S. A., Rio de Janeiro.
- Wooley, G.R., 1980. “Computing downhole temperatures in circulation, injection and production wells”. *Journal of Petroleum Technology*, pp. 1509–1522.

7. RESPONSIBILITY NOTICE

The authors are the only responsible for the printed material included in this paper.